Nature of the Long-Range Structural Changes Induced by the Molecular Photoexcitation and by the Relaxation in the Prussian Blue Analogue $Rb_{1.8}Co_4[Fe(CN)_6]_{3.3}\cdot 13H_2O$. A Synchrotron X-ray Diffraction Study

V. Escax,[†] A. Bleuzen,*[,†] J. P. Itié,[‡] P. Munsch,[‡] F. Varret,[§] and M. Verdaguer[†]

Laboratoire de Chimie Inorganique et Matériaux Moléculaires, Unité CNRS 7071, Université Pierre et Marie Curie, Bat F 74, 4 place Jussieu, 75252 Paris Cedex 05, France, Laboratoire pour 1'Utilisation du Rayonnement Electromagnétique, UMR CNRS 130-CEA-MENRS, Bat 209d, Université Paris-sud. BP34, 91898 Orsay Cedex, France, and Laboratoire de Magnétisme et d'Optique, CNRS, Université de Versailles (UMR 8634), 45 avenue des Etats-Unis, 78035 Versailles Cedex, France

Received: January 7, 2003

The photomagnetic properties of CoFe Prussian blue analogues arise from a photoinduced $Co^{III}(LS)-Fe^{II}(LS) \rightarrow Co^{II}(HS)-Fe^{III}(LS)$ [LS = low spin, HS = high spin] electron transfer accompanied by a spin state change of the cobalt and a significant expansion of the cobalt coordination sphere. The local bond-lengthening around the cobalt induces long-range structural changes that we studied by X-ray powder diffraction using synchrotron radiation. Beyond the structural characterization of an excited metastable state, the study shows how a photoinduced molecular bond-lengthening is made possible in a face-centered cubic Prussian blue analogue by the presence of $[Fe(CN)_6]$ vacancies: in their vicinity, the lengthening of the cobalt to ligands bonds is easier. The excitation process starts at the cobalt neighbors of the vacancies through a continuous or second-order transformation (in a single phase), which triggers a cooperative propagation through a first-order discontinuous transition (between two phases).

Introduction

Since the evidence of a photomagnetic CoFe Prussian blue analogue by Hashimoto and co-workers in 1996,[1,2] the interest for photomagnetic Prussian blue derivatives is growing.[3−5] Up to now the CoFe analogues have been the most studied. Hashimoto et al. have synthesized compounds exhibiting spectacular properties,[1,6−10] Miller et al. have investigated the magnetic properties of the excited metastable state on the basis of dynamic studies.[11,12] We undertook a systematic study to understand the scope and the mechanism of the phenomenon.[13−17] In previous works, we synthesized compounds showing the importance of the cobalt ion ligand field strength and of the network flexibility. We obtained the efficient compound, $Rb_{1.8}Co^{III}_{3.3}Co^{II}_{0.7}[Fe(CN)_6]_{3.3}[\ ]_{0.7}\cdot 13H_2O$[14] named $Rb_{1.8}Co_4Fe_{3.3}$ in the following, in which we evidenced the electronic structure and the local structure changes[15] involved in the photomagnetic properties. At low temperature, an irradiation in the visible range produces an electron transfer associated with a spin crossover of the cobalt ion $Co^{III}(LS)-Fe^{II}(LS) \rightarrow Co^{II}(HS)-Fe^{III}(LS)$ and modifies the magnetic properties:[17] the compound, initially practically diamagnetic, undergoes a diamagnetic−ferrimagnetic transition with a Curie temperature at 21 K. This electron transfer is accompanied by an important lengthening (0.18 Å) of the cobalt to first neighbors bonds due to the population of the cobalt ion e_g^* antibonding orbitals in the $Co^{III}(LS)$ ($t_{2g}^6eg^0$) to $Co^{II}(HS)$ ($t_{2g}^5e_g^2$) process. The bond lengthening is made possible by the network flexibility due to the presence of $[Fe(CN)]_6$ vacancies in the centered cubic structure (fcc). This photoinduced electron transfer is reversible $Co^{II}(HS)-Fe^{III}(LS) \rightarrow Co^{III}(LS)-Fe^{II}(LS)$ when heating the sample above the relaxation temperature (110 K).[9,18,19] The lifetime of the excited metastable state depends on the temperature: the closer to the relaxation temperature the temperature is, the shorter the lifetime is. The transformation back to the ground state is, on the contrary, accompanied by a shortening of the cobalt first neighbors bonds from $Co^{II}(HS)$ to $Co^{III}(LS)$. The expansion of the cobalt coordination sphere during the excitation process or its reduction during the relaxation process are expected to produce long-range order changes. To study these changes, we performed X-ray powder diffraction using synchrotron radiation at low temperature (10 K) under continuous irradiation during the excitation process, and then for increasing temperature after irradiation in the course of the relaxation process.

Property changes under external strains have been extensively studied in spin crossover compounds, especially in the course of thermoinduced spin crossover.[20−24] Structural changes have also been investigated.[25−31] Two different kinds of transitions were evidenced: (1) second-order, i.e., continuous transformations, which show a gradual variation of the physical properties associated with a continuous change of the structural parameters of a same phase (shift of the Bragg reflections for example); (2) first order, i.e., discontinuous transitions, characterized by an abrupt change of the relevant physical properties associated with different structural phases (coexistence of the individual X-ray diffraction patterns of the two phases associated with the two spin states, for example). The mechanisms involved in such kind of transformations are complex and are not yet completely understood.

* To whom correspondence should be addressed. Fax: +33-1-44-27-38-41. Telephone: +33-1-44-27-32-77. E-mail: bleuzen@ccr.jussieu.fr.
[†] Université Pierre et Marie Curie.
[‡] Laboratoire pour l'Utilisation du Rayonnement Electromagnétique.
[§] Université de Versailles.

10.1021/jp0340313 CCC: $25.00
Published on Web 04/29/2003

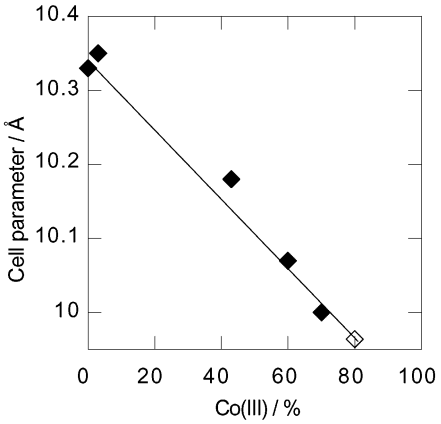

Figure 1. Cell parameter in the $Cs_xCo_4Fe_{(x+8)/3}$ series (close squares) and for $Rb_{1.8}Co_4Fe_{3.3}$ (open squares) as a function of the Co^{III}(LS) percentage at room temperature.

To go further in the analysis of the X-ray diffraction of the $Rb_{1.8}Co_4Fe_{3.3}$ compound under strains, the diffraction patterns were compared to those of a series of CoFe Prussian blue analogues that we previously synthesized and characterized.[16] In this series, we progressively fill the tetrahedral sites of the fcc structure by cesium cations. By control of the amount of cesium cations in the structure, the average ligand field strength around the cobalt ion and the Co^{III}/Co^{II} redox potentiel can be finely tuned. As a consequence, during the synthesis, more and more $Co^{II}-Fe^{III}$ pairs are transformed into $Co^{III}-Fe^{II}$ ones as the cesium amount increases through a Co^{II}(HS)$-Fe^{III}$(LS) $\rightarrow$ Co^{III}(LS)$-Fe^{II}$(LS) charge transfer. Each compound represents one of the stages in the transformation from Co^{III}(LS)$-Fe^{II}$(LS) to Co^{II}(HS)$-Fe^{III}$(LS). As the states are chemically frozen, it is possible to study each of them by different techniques. The X-ray diffraction patterns of the compounds of the $Cs_xCo_4Fe_{(x+8)/3}$ series are characteristic of a fcc lattice. For each reflection, only one peak appears. Its position, intensity, and line width vary along the series. The broadening and the collapsing of the peaks reflect the disorder due to the coexistence of long $Co^{II}-$ligand bonds and short $Co^{III}-$ligand bonds within the same fcc phase. When the system is mainly composed of Co^{II}(HS) or Co^{III}(LS), the peaks are intense and narrow. The progressive substitution of one of the species by the other produces the broadening and the collapsing of the peaks up to a composition close to 50% in Co^{II}(HS) and 50% in Co^{III}(LS). The cell parameter reflects the electronic state of the cobalt atoms in the structures (Figure 1): it is a linear function of the amount of Co^{III}(LS) species in the compounds in a wide range of concentration.

The X-ray diffraction pattern of $Rb_{1.8}Co_4Fe_{3.3}$ where 80% of the cobalt ions are low spin Co^{III}, is characteristic of a fcc structure and its cell parameter $a = 9.96 \pm 0.05$ Å fits the linear variation (Figure 1). Those results are used in the present paper to understand the nature of the long-range order modifications in the course of the photoinduced electron transfer and the relaxation processes.

Experimental Section

Synchrotron X-ray Diffraction. Energy-dispersive X-ray diffraction patterns were recorded over the 0.5−70 keV energy range on the DW-11A energy-dispersive X-ray beamline on the DCI ring of the LURE synchrotron facility in Orsay, France. The orientation of the detector was fixed at $\theta = 3.925°$ and measured using the EDXD (energy dispersive X-ray diffraction) pattern of a Cu foil at ambient temperature. The powder was spread on between two tapes. At low temperature, the white X-ray beam induces the Co^{III}(LS)$-Fe^{II}$(LS) to Co^{II}(HS)$-Fe^{III}$(LS) electron transfer. It has already been mentioned that it is possible to trap spin states using X-rays.[32]

The X-ray source being the probe beam as well as the pumping beam makes sure that the whole diffracting sample has been irradiated. Such experimental conditions allow one to avoid the problem of the penetration depth of light in a dark powdered sample. The measure concerns the irradiated part of the sample only. The reason some Co^{III}(LS)$-Fe^{II}$(LS) pairs would not be phototransformed may not be due to a lack of photons.

In a first step, the study of the excitation process was carried on under continuous irradiation. X-ray powder diffraction patterns were recorded as a function of the irradiation time. The acquisition time was 30 s, except for the first point (15 s). During this time the pattern change is unobservable.

In a second step, the relaxation process was studied by increasing the temperature after an irradiation time of 1 h at 10 K. X-ray powder diffraction patterns were recorded as a function of temperature. For this part of the study, the X-ray beam was switched on only for the measurement. The acquisition time was 15 s. The measurement was repeated three times at the same temperature without detectable change of the pattern.

The energy position, line width and intensity were obtained by fitting the peaks to Gaussian line shape. Two reflections, the 200 and 220 were intense enough to work with. The changes in the peak profile as a function of irradiation time or temperature were comparable for all the reflections. We choose therefore, for clarity, to present the results for the 220 reflection only. The resolution in energy is poorer for the 200 one. For the variable temperature measurements, the photoinduced patterns changes exceed by far the thermal changes, which were neglected.

Materials and Sample Preparation. $Rb_{1.8}Co_4Fe_{3.3}$ studied here is synthesized by precipitation in solution in the presence of an excess of rubidium cations.[14] The powder crystallizes in cubic system, fcc network. The chemical formula for one conventional cell is $Rb_{1.8}Co^{III}_{3.3}Co^{II}_{0.7}[Fe^{II}(CN)_6]_{3.3}[\ ]_{0.7}\cdot 13H_2O$ ([ ] represents a $[Fe^{II}(CN)_6]$ vacancy). The compounds of the $Cs_xCo_4Fe_{(x+8)/3}$ series are prepared by precipitation from solutions containing different amounts of cesium cations.[16] All the powders crystallize in the fcc network. The formulas for one conventional cell are $K_{0.1}Co_4[Fe(CN)_6]_{2.7}[\ ]_{1.3}\cdot 18H_2O$, $Cs_{0.3}Co_4[Fe(CN)_6]_{2.8}[\ ]_{1.2}\cdot 18H_2O$, $Cs_{0.7}Co_4[Fe(CN)_6]_{2.9}[\ ]_{1.1}\cdot 16H_2O$, $Cs_{1.3}Co_4[Fe(CN)_6]_{3.2}[\ ]_{0.8}\cdot 16H_2O$, $Cs_{2.3}Co_4[Fe(CN)_6]_{3.4}[\ ]_{0.6}\cdot 14H_2O$, and $Cs_{3.9}Co_4[Fe(CN)_6]_{3.9}[\ ]_{0.1}\cdot 13H_2O$.

Results and Discussion

We analyze hereunder, independently, the energy position, the intensity, and line width of the 220 reflection as a function of irradiation time and temperature. We compare then the data to the ones of the $Cs_xCo_4Fe_{(x+8)/3}$ series at room temperature, which allows to better understand the phenomena.

Peak Profile. The X-ray diffraction patterns of $Rb_{1.8}Co_4Fe_{3.3}$ under irradiation at 10 K over the 16−27 keV energy range are displayed for increasing irradiation time in Figure 2a. After 1 h of irradiation, the photoexcitation is achieved, and the patterns are recorded for increasing temperature. They are displayed in Figure 2b.

Increasing irradiation time (Figure 2a) produces first the broadening of the initial 220 diffraction line and then the growth of a new peak shifted to lower energy. After 1 h under irradiation, the initial peak has almost disappeared, so only the lower energy peak remains. The increase of the temperature

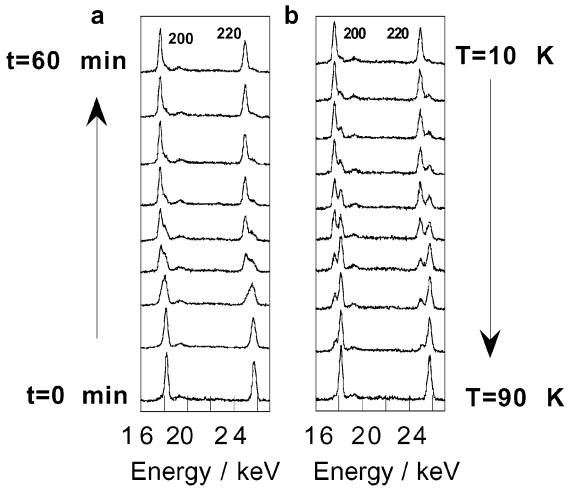

Figure 2. X-ray powder diffraction patterns of $Rb_{1.8}Co_4Fe_{3.3}$: (a) at 10 K under continuous irradiation (excitation process); (b) as a function of temperature (thermal relaxation process).

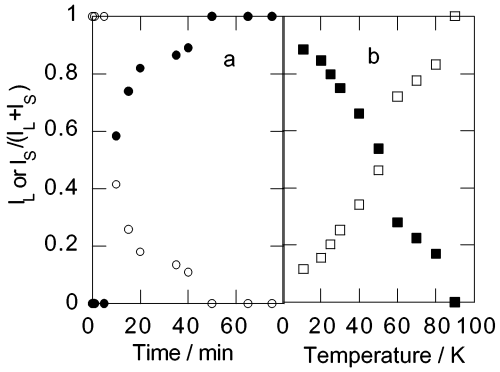

Figure 3. Relative intensities of the 220 diffraction lines corresponding to the S and L phases of $Rb_{1.8}Co_4Fe_{3.3}$: (a) at 10 K as a function of irradiation time (photoexcitation process: open circles, S phase; close circles, L phase); (b) as a function of temperature (thermal relaxation process: open squares, S phase; close squares, L phase).

(Figure 2b) after 1 h under irradiation leads to the progressive decay of the lower energy peak and the growth of the higher energy one. At 90 K, only the peak at higher energy remains, identical to the initial peak before irradiation. 90 K is the temperature corresponding to a complete thermal relaxation as expected from magnetism.

It is noticeable that the two diffraction peaks are more resolved during the relaxation process than during the excitation process. This means that whereas the phenomenon, as a whole, is reversible, the structural change is different during the photoexcitation and the thermal relaxation.

The new peak situated at lower energy is the signature of a new fcc phase with a longer cell parameter. In the following, the two phases will be called S for the phase with the shorter cell parameter and L for the phase with the longer cell parameter.

The presence of two well-resolved peaks reflects the existence of two kinds of diffracting domains. The domains forming the S phase are mainly composed of Co^{III}(LS) ions with short cobalt to ligands bonds. The others form the L phase mainly composed of Co^{II}(HS) ions with long cobalt to ligands bonds. The variations with time and with temperature of the relative intensities of the S and L phases $I_S/(I_S + I_L)$ and $I_L/(I_S + I_L)$ (Figure 3, parts a and b, respectively) expresses the change of the quantity of both phases in the sample. These observations are characteristic of a first-order, or discontinuous, transition.

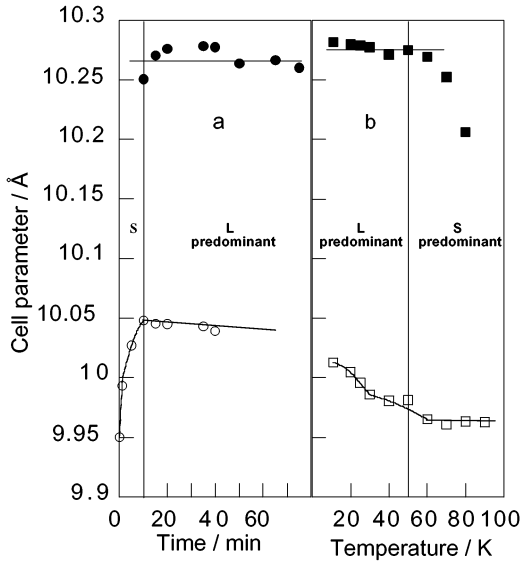

Figure 4. Cell parameter of the S and L phases of $Rb_{1.8}Co_4Fe_{3.3}$: (a) at 10 K as a function of irradiation time (photoexcitation process: open circles, S phase; close circles, L phase); (b) as a function of temperature (thermal relaxation process: open squares, S phase; close squares, L phase).

Energy Position. The average cell parameters a_S and a_L deduced from the energy position of the diffraction peaks are displayed for increasing irradiation time during the excitation process in Figure 4a and for increasing temperature during the relaxation process in Figure 4b.

During the first 10 min of irradiation, the cell parameter of the initial phase (S) significantly and continuously increases (open circles, Figure 4a, bottom). This behavior is the signature of a continuous Co^{III}(LS) → Co^{II}(HS) photoinduced transformation. Once the second peak with a higher cell parameter corresponding to the L phase appears, the cell parameters of both phases remain practically constant (close circles, Figure 4a, top). Only the relative intensity of the peaks varies (Figure 3a). S domains are transformed into L domains. This behavior is the signature of a discontinuous S → L photoinduced transition.

During the relaxation process, over the 10−50 K temperature range (Figure 4b), the cell parameter of the L phase remains practically constant (close squares, Figure 4b, top). Only the relative intensity of the peaks corresponding to the S and L phases varies (Figure 3b). L domains are transformed into S domains. This behavior is the signature of a discontinuous L → S thermoinduced transition.

Over the same temperature range, the S phase grows (Figures 2b and 3b) and its cell parameter significantly and continuously decreases (open squares, Figure 4b, bottom). The S phase undergoes a continuous Co^{II}(HS) → Co^{III}(LS) thermoinduced transformation.

Above 50 K, the cell parameter of the S phase is constant which indicates that the phase is completely relaxed (open squares, Figure 4b, bottom). The S phase is now the predominant one (Figure 3b). The L phase cell parameter remains practically unchanged up to 60 K (close squares, Figure 4b, top). Over the 60−80 K temperature range, at the time when the L phase disappears, its cell parameter significantly and continuously decreases: the L phase undergoes a continuous Co^{II}(HS) → Co^{III}(LS) thermoinduced transformation.

At 90 K, the relaxation back to the ground state is achieved, the initial structure is recovered.

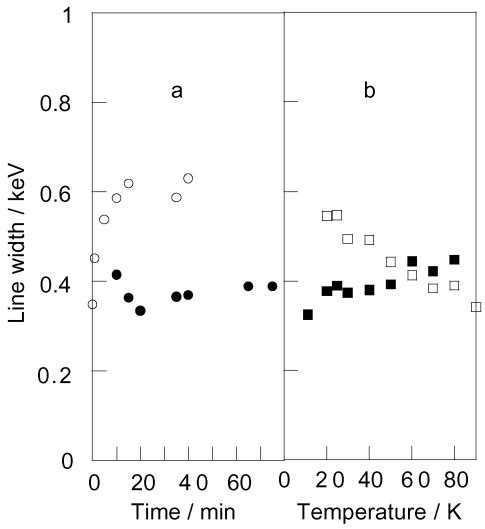

Figure 5. Line width of the peaks corresponding to the S and L phases of $Rb_{1.8}Co_4Fe_{3.3}$: (a) at 10 K as a function of irradiation time (photoexcitation process: open circles, S phase; close circles, L phase); (b) as a function of temperature (thermal relaxation process: open squares, S phase; close squares, L phase).

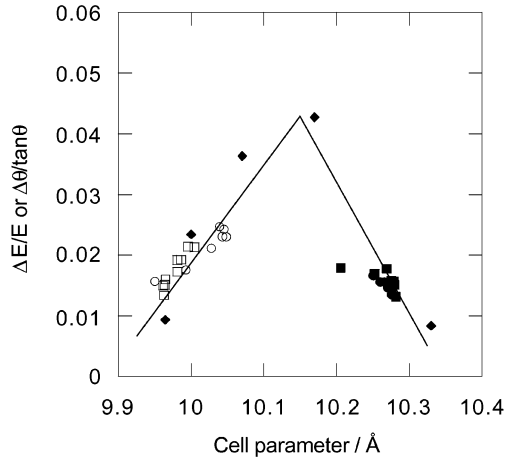

Figure 6. Reduced line widths ($\Delta E/E$) as a function of the cell parameter of $Rb_{1.8}Co_4Fe_{3.3}$ during photoexcitation (open circles, S phase; close circles, L phase) and during thermal relaxation (open squares, S phase; close squares, L phase) and reduced line widths ($\Delta\theta/\tan\theta$) as a function of the cell parameter along the $Cs_xCo_4Fe_{(x+8)/3}$ series.

Line Width. The line widths of the S and L phases (LW_S and LW_L) as a function of irradiation time and of temperature are respectively shown in Figure 5, parts a and b.

The variation of the line widths of the peaks with irradiation time or temperature (Figure 5) is strongly correlated to the variation of the cell parameter of the corresponding phases. The more the value of the cell parameter deviates from the ones of a pure Co^{II}(HS) or Co^{III}(LS) phase, the broader the peak is. This correlation was already observed along the $Cs_xCo_4Fe_{(x+8)/3}$ series. The variation of the line width $\Delta E/E$ during the photoexcitation and the thermal relaxation of $Rb_{1.8}Co_4Fe_{3.3}$ and the variation of $\Delta\theta/\tan\theta$ along the $Cs_xCo_4Fe_{(x+8)/3}$ series as a function of the cell parameter are shown in Figure 6.

At first glance, $\Delta E/E$ for $Rb_{1.8}Co_4Fe_{3.3}$ (either for photoexcitation or for thermal relaxation) and $\Delta\theta/\tan\theta$ along the $Cs_xCo_4Fe_{(x+8)/3}$ series follow the same trend. The points, except for one of them, are situated on two straight lines: one with a positive slope, one with a negative slope. The origin of the diffraction lines broadening is then the same in both cases. The broadening reflects the structural disorder due to the coexistence

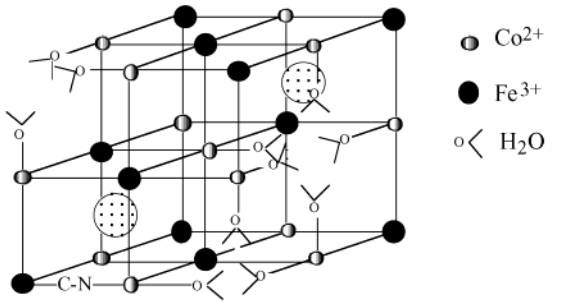

Figure 7. Scheme of a unit cell of the $Rb_{1.8}Co_4Fe_{3.3}$ compound.

of short Co^{III}(LS)−ligand bonds and long Co^{II}(HS)−ligand bonds within the same fcc structure. The two lines intersect around a cell parameter value of 10.15 Å. The percentage of Co^{III} ions in the structure corresponding to the maximum, deduced from Figure 1, is approximately 50%, the composition expected for the most disordered structure.

The crucial difference between the $Rb_{1.8}Co_4Fe_{3.3}$ compound under external strains and the $Cs_xCo_4Fe_{(x+8)/3}$ series lies in the amplitude of the variations of the lines broadening. The points are spread over the whole cell parameter range along the $Cs_xCo_4Fe_{(x+8)/3}$ series: the progressive substitution of Co^{II}(HS) ions with long metal to ligand bonds by Co^{III}(LS) ions with short metal to ligand bonds produces on the X-ray diffraction pattern the progressive shift and broadening of the unique 220 diffraction line.

The behavior is related to a continuous Co^{II}(HS) → Co^{III}(LS) chemically induced transformation. This is a typical behavior of solid solutions.

On the contrary, for $Rb_{1.8}Co_4Fe_{3.3}$, the points are situated over well-delimited cell parameter ranges, different for photoexcitation and thermal relaxation. The discontinuity is associated with the coexistence of two discrete phases and to the S → L (excitation) and L → S (relaxation) discontinuous transitions.

The cell parameter variation range of one phase (S, L or the whole compound in the $Cs_xCo_4Fe_{(x+8)/3}$ series) reflects a Co^{II}(HS) → Co^{III}(LS) continuous transformation occurring within this phase. Thus, Figure 6 clearly shows that the amplitude of the continuous transformation in $Rb_{1.8}Co_4Fe_{3.3}$ is more important within the S than within the L phase. The points corresponding to the L phase are concentrated on a very limited zone of the curve, whereas the points corresponding to the S phase are spread over a limited but larger zone. In fact, the L phase cell parameter are nearly concentrated on one point which indicates a nearly fixed electronic state within this phase, whereas the cell parameter of the S phase varies from 9.96 to 10.05 Å, which corresponds to a Co^{III}(LS) ions content ranging from 80% to 60%, according to Figure 1. This can be explained in light of the structure of the compound (Figure 7).

For the first time, the irradiation produces in the initial S phase the excitation of randomly distributed Co^{III}(LS) species associated with a local continuous transformation. These species are easily excited, they must be situated next to $[Fe(CN)]_6$ vacancies. The process involves 20% (80%−60%) of the cobalt ions initially at the +III oxidation state. This amount of cobalt ions represents 0.8 cobalt ion in a unit cell, which is very close to the amount of $[Fe(CN)]_6$ vacancy per unit cell (0.7) as if each $[Fe(CN)]_6$ vacancies, acting as relaxation points of the strains, allowed the excitation or the cobalt−ligand bond lengthening of one cobalt ion. At the time when 20% of the cobalt ions easy to excite are transformed, the interactions between the excitable species become stronger, leading to cooperative or auto-accelerated effects with the formation of L

domains through a S → L discontinuous transition. Extensive stable L domains are then created with a quite well-defined electronic state.

During the thermal relaxation two processes occur simultaneously: the L → S discontinuous transition leading to more resolved diffraction lines than during the excitation process (Figure 2) and the $Co^{II}(HS) \rightarrow Co^{III}(LS)$ continuous transformation within the S phase leading to the progressive decrease of the S phase cell parameter value (Figure 4b, bottom). The L domains relax over the 10−90 K temperature range depending on the strength of macroscopic network strains whereas, the remaining Co^{II} species next to $[Fe(CN)]_6$ vacancies belonging to the S phase relax over the 10−50 K temperature range depending on the Co^{II} ion local environment.

The only point outside the correlation (Figure 6) corresponds to the last point before the disappearance of the L phase during the relaxation process. At this time, the proportion of L domains is vanishing. Those domains would undergo unusually strong network strains, which would produce a continuous transformation with a structural evolution different from that observed in the rest of the series of points.

Conclusion

To our knowledge, this is the first structural study carried out in the course of a photoinduced electron transfer accompanied by a spin state change in a three-dimensional compound.

Studies of spin crossover compounds show the complexity of the phenomenon, the importance of the phonons interactions in the crystal and the extreme sensitivity of the transition to tiny structural changes (substituents on the ligands, solvent, deuteriation...).[30,31,33]

In $Rb_{1.8}Co_4Fe_{3.3}$, continuous and discontinuous transformations simultaneously happen in the course of the photoexcitation and of the relaxation processes, associated with weak and strong vibrational interactions between the metallic centers. The interactions between excitable centers linked through CN ligands are probably stronger than the other interactions and dominate all the other effects. More generally, in the $C_xCo_4Fe_{(8+x)/3}$ Prussian blue derivatives, the structural changes will depend intimately on the Co^{II}/Co^{III} ratio, the amount of $[Fe(CN)_6]$ vacancies, and the nature of the alkali cation. A study as a function of the stoichiometry and the nature of the inserted alkali cation in the same family of compounds is in progress.

Acknowledgment. We thank the European Community (Grant ERBFMRXCT980181), Contract TMR/TOSS (FMRX-CT98-0199), and the CNRS (Programme Matériaux) for financial support.

References and Notes

(1) Sato, O.; Iyoda, T.; Fujishima, A.; Hashimoto, K. *Science* **1996**, *272*, 704−705.Sato, O.

(2) Verdaguer, M. *Science* **1996** , *272*, 698−699.

(3) Rombault, G.; Verelst, M.; Gohlen, S.; Ouahab, L.; Mathonière, C.; Kahn, O. *Inorg. Chem.* **2001**, *40*, 1151−1159.

(4) Ohkoshi, S.-I.; Hashimoto, K. *J. Photochem. Photobiol.* **2001**, *2*, 71−88.

(5) Ohkoshi, S.-I.; Yorosu, S.; Sato, O.; Iyoda, T.; Fujishima, A.; Hashimoto, K. *Appl. Phys. Lett.* **1997**, *70*, 1040−1042.

(6) Sato, O.; Einaga, Y.; Iyoda, T.; Fujishima, A.; Hashimoto, K. *J. Electrochem. Soc.* **1997**, *144*, L11−L13.

(7) Sato, O.; Einaga, Y.; Iyoda, T.; Fujishima, A.; Hashimoto, K. *J. Phys. Chem. B* **1997**, *101*, 3903−3905.

(8) Einaga, Y.; Ohkoshi, S.-I.; Sato, O.; Fujishima, A.; Hashimoto, K. *Chem. Lett.* **1998**, 585−586.

(9) Sato, O.; Einaga, Y.; Fujishima, A.; Hashimoto, K. *Inorg. Chem.* **1999**, *38*, 4405−4412.

(10) Shimamoto, N.; Ohkoshi, S.; Sato, O.; Hashimoto, K. *Inorg. Chem.* **2002**, *41*, 678−684.

(11) Pejacovic, D. A.; Manson, J. L.; Miller, J. S. *J. Appl. Phys.* **2000**, *87*, 6028−6030.

(12) Pejacovic, D. A.; Manson, J. L.; Miller, J. S. *Phys. Rev. Lett.* **2000**, *85*, 1994−1997.

(13) Bleuzen, A.; Lomenech, C.; Dolbecq, A.; Villain, F.; Goujon, A.; Roubeau, O.; Nogues, M.; Varret, F.; Baudelet, F.; Dartyge, E.; Giorgetti, C.; Gallet, J. J.; Cartier dit Moulin, C.; Verdaguer, M. *Mol. Cryst. Liq. Cryst.* **1999**, *335*, 965−974.

(14) Bleuzen, A.; Lomenech, C.; Escax, V.; Villain, F.; Varret, F.; Cartier dit Moulin, C.; Verdaguer, M. *J. Am. Chem. Soc.* **2000**, *122*, 6648−6652.

(15) Cartier dit Moulin, C.; Villain, F.; Bleuzen, A.; Arrio, M.-A.; Sainctavit, P.; Lomenech, C.; Escax, V.; Baudelet, F.; Dartyge, E.; Gallet, J. J.; Verdaguer, M. *J. Am. Chem. Soc.* **2000**, *122*, 6653−6658.

(16) Escax, V.; Bleuzen, A.; Cartier dit Moulin, C.; Villain, F.; Goujon, A.; Varret, F.; Verdaguer, M. *J. Am. Chem. Soc.* **2001**, *123*, 12536−12543.

(17) Champion, G.; Escax, V.; Cartier dit Moulin, C.; Bleuzen, A.; Villain, F.; Arrio, M.-A.; Baudelet, F.; Dartyge, E.; Verdaguer, M. *J. Am. Chem. Soc.* **2001**, *123*, 12536−12543.

(18) Goujon, A.; Roubeau, O.; Varret, F.; Dolbecq, A.; Bleuzen, A.; Verdaguer, M. *Eur. Phys. J. B* **2000**, *14*, 115−124.

(19) Goujon, A.; Varret, F.; Escax, V.; Bleuzen, A.; Verdaguer, M. *Polyhedron* **2001**, *20*, 1347−1354.

(20) Goodwin, H. A. *Coord. Chem. Rev.* **1976**, *18*, 293.

(21) Gütlich, P. *Struct. Bonding (Berlin)* (berlin) **1981**, *44*, 83.

(22) König, E. *Prog. Inorg. Chem.* **1987**, *35*, 527.

(23) Toflund, H. *Coord. Chem. Rev.* **1989**, *94*, 67−108.

(24) Gütlich, P.; Hauser, A. *Coord. Chem. Rev.* **1990**, *97*, 1.

(25) Gütlich, P.; Hauser, A.; Spiering, H. *Angew. Chem., Int. Ed. Engl.* **1994**, *337*, 2024.

(26) König, E.; Watson, K. *J. Chem. Phys. Lett.* **1970**, *6*, 457.

(27) Katz, B. A.; Strouse, C. E. *J. Am. Chem. Soc.* **1979**, *101*, 6214.

(28) Cecconi, F.; DiVaira, M.; Middollini, S.; Orlandini, A.; Sacconi, L. *Inorg. Chem.* **1981**, *20*, 3423.

(29) König, E.; Ritter, G.; Dengler, J.; Thuéry, P.; Zarembowitch, J. *Inorg. Chem.* **1989**, *28*, 1757−1759.

(30) Guionneau, P.; Létard, J.-F.; Yufit, D. S.; Chasseau, D.; Bravic, G.; Goeta, A. E.; Howard, J. A. K.; Kahn, O. *J. Mater. Chem.* **1999**, *9*, 985−994.

(31) Jung, J.; Schmitt, L.; Wiehl, L.; Hauser, A.; Knorr, K.; Spiering, H.; Gütlich, P. *Z. Phys. B* **1996**, *100*, 523−534.

(32) Collison, D.; Garner, C. D.; McGrath, C. M.; Mosselmans, J. F. W.; Roper, M. D.; Seddon, J. M. W.; Sinn, E.; Young, N. A. *J. Chem. Soc., Dalton Trans.* **1997**, 4371.

(33) Jeftic, J.; Hauser, A. *J. Phys. Chem. B* **1997**, *101*, 10262−10270.

(34) Sorai, M.; Seki, S. *J. Phys. Chem. Solids* **1974**, *35*, 555−570.